Available online at www.sciencedirect.com
SCIENCE DIRECT®
International Journal of Hydrogen Energy 31 (2006) 603–611
International Journal of HYDROGEN ENERGY
www.elsevier.com/locate/ijhydene

The self-discharge mechanism of AB_5-type hydride electrodes in Ni/MH batteries

Chunsheng Wang[a,*], Mariza Marrero-Rivera[b], Daniel A. Serafini[b], Jack H. Baricuatro[b], Manuel P. Soriaga[b], Supramaniam Srinivasan[c,✠]

[a]*Center for Manufacturing Research and Department of Chemical Engineering, Tennessee Technological University, Cookeville, TN 38505, USA*
[b]*Department of Chemistry, Texas A& M University, College Station, TX 77843, USA*
[c]*Center for Energy and Environmental Studies, Princeton University, Princeton, NJ 08544, USA*

Received 1 November 2004; received in revised form 1 May 2005
Available online 9 August 2005

Abstract

A new strategy in the study of the self-discharge mechanism of metal-hydride electrodes has been developed. The self-discharge behavior of a $LaNi_{3.55}Co_{0.75}Mn_{0.4}Al_{0.3}$ electrode in alkaline solution, with and without ZnO additive, was investigated. Experimental results showed that the self-discharge rate (hydrogen desorption) within the single-phase region is controlled by the difference between the equilibrium hydrogen partial pressure at the electrode and the actual hydrogen partial pressure in the cell. Dissolved oxygen was also found to exert a strong influence on the self-discharge rate in the single-phase region. In the two-phase region, the self-discharge is limited by the rate of phase transformation. A four-step mechanism for the self-discharge process is proposed.

Keywords: Ni-metal-hydride batteries; Metal-hydride electrodes; Hydrogen storage; Phase transformation; Self-discharge

1. Introduction

The numerous advantages of nickel–metal-hydride (Ni/MH) batteries, based on a hydrogen storage alloy as the anode, over Ni/Cd batteries are well established. Among these advantages are: higher energy density and power, longer cycle life, and the capability of over-charge and over-discharge [1]. However, the rate of self-discharge of Ni/MH batteries is known to be higher than that of Ni/Cd batteries.

The self-discharge mechanism of Ni/MH batteries has been widely investigated [2,3]. The high self-discharge rate of sealed Ni/MH batteries is thought to result from the shuttle reactions between the nitrite ions and ammonia emanating from decomposition reactions at the separating membrane [2,3]. There is, however, a lack of clear understanding of the self-discharge characteristics of the MH electrode itself which limits the optimal performance of Ni/MH batteries.

It has been reported [4] that capacity losses can be reversible or irreversible. Reversible capacity losses result from the desorption of hydrogen from the hydride anode, while irreversible capacity losses are due to the degradation of the hydride anode itself. Other investigators have found that the difference between the prevailing partial

✠Deceased
* Corresponding author. Tel.: +1 931 372 3678; fax: +1 931 372 6345.
E-mail addresses: cswang@tntech.edu (C. Wang), m-soriaga@tamu.edu (M.P. Soriaga).

0360-3199/$30.00
doi:10.1016/j.ijhydene.2005.06.001

pressure of hydrogen around the MH electrode and the equilibrium partial pressure controls the hydrogen evolution from the MH electrode and thus, determines the self-discharge rate of anodes such as $Zr_{1-x}Ti_xV_{0.8}Ni_{1.6}$ [5] and $MmNi_{3.3+x}Co_{0.7}Al_{1.0-x}$ [6]. Electrodes with higher equilibrium hydrogen pressure are found to have higher self-discharge rates [5,6].

More recent results [7] showed that the self-discharge behavior of the $V_{0.9}Ti_{0.1}$ alloy in an open cell is attributable to the desorption of hydrogen at both the high-plateau pressure (0.1 atm) and the low-plateau pressure (10^{-8} atm, lower than the partial pressure of hydrogen in air). The self-discharge rate of the $V_{0.9}Ti_{0.1}$ electrode was shown not to be completely suppressed by the reduction of the plateau pressure of the alloy. This implies that there are other factors, in addition to the hydrogen pressure difference, which affect the self-discharge rates of MH electrodes.

In a sealed NiMH cell, hydrogen partial pressure depends on the free space in the cell and the hydrogen oxidation ability of MH electrode. The oxidation is promoted in an over-charge process to reduce the internal oxygen pressure of the cell and avoid hydrogen gas accumulation. Since the oxygen diffusion in the electrolyte is slow and its solubility is low, the hydrogen and oxygen recombination process is very closely related to the amount of electrolyte. When the electrode assembly is over wetted, the recombination process is slow, an indication that the electrolyte is a barrier for the oxidation reaction.

Usually, the self-discharge rate of hydride electrodes is measured from the charge retention at different open-circuit times. The charge retention measurements at different rest times are carried out in the following sequence: (i) a full charge of the electrode, (b) equilibration (rest) at pre-selected times, followed by a discharge at a low rate (0.2–0.25 C). Unfortunately, the charge retention at a short time interval cannot be accurately measured due to the decrease in the capacities with charge/discharge cycles (i.e., irreversible capacity loss) [4]. Moreover, the entire measurement lasts for a long period.

In this paper, we describe a novel, facile procedure to measure the self-discharge (hydrogen desorption) rate of hydride electrodes in the open and partially sealed cells. To simulate the self-discharge of MH electrodes in a sealed Ni/MH cell, the influence of the oxidation of adsorbed hydrogen by dissolved oxygen (DO), as well as the rate of phase transformation on the self-discharge behavior, was also studied. A new self-discharge mechanism of hydride electrodes is proposed.

2. Experimental

2.1. Preparation of the alloy

Alloy ingots of $LaNi_{3.55}Co_{0.75}Mn_{0.4}Al_{0.3}$ were prepared by arc-melting a mixture of La, Ni, Co, Mn, and Al under He atmosphere and then annealing for 72 h. The ingots were pulverized into a powder with a mean diameter of 10 μm by gas-phase hydrogen absorption and desorption cycles. The crystal structure was examined by X-ray diffraction (XRD). For the electrochemical measurements, electrodes were prepared by mixing alloy powder and binder in a 50:50 weight ratio. This mixture was pressed onto a nickel mesh at a pressure of 300 kg/cm^2. The binder used was carbon (Vulcan-XC-72) with 33% polytetrafluoroethylene. The working electrode contained 75 mg of active alloy and had a surface area of 2 cm^2. The counter electrode was made of a Ni mesh with a surface area approximately 10 times that of the working electrode. Both flooded and partially opened (loosely capped) cells were employed and coupled to a Luggin capillary for a Hg/HgO reference electrode. The electrolyte was either 6 M KOH or 0.5 M ZnO in 6 M KOH. The purpose of ZnO addition into the 6 M KOH electrolyte is to decrease the corrosion of the MH electrode [8,9]. Electrochemical measurements were carried out after full charge/discharge activation with an automatic battery cycler (Arbin Corporation, College Station, TX). XRD patterns were obtained using a Rigaku AFC5 diffractometer equipped with a rotating anode operated at 50 KV and 180 mA with a Cu target and graphite monochromation.

2.2. Isotherms of $LaNi_{3.55}Co_{0.75}Mn_{0.4}Al_{0.3}$

After 80 charge–discharge cycles, electrodes were charged with a current of 50 mA/g for 5 h; the equilibrium discharge potential-composition-isotherms (PCI) at room temperature were then generated by the following alternating processes: (i) application of a pulse discharge of 25 mA/g for 0.33 h, and (ii) equilibration (rest) for 0.33 h until a constant potential was attained. The concentration and equilibrium pressure of hydrogen are obtained from the PCI curves using the following equations [10]:

$$x = \frac{wQ_d}{F} = \frac{421.53Q_d}{26800}, \quad (1)$$

$$P_{H_2} = 10^{-(0.93045+E)/0.029547}, \quad (2)$$

where x is the ratio of the number of moles of hydrogen with respect to the number of moles of the metal, Q_d discharge capacity in mAh/g, w the weight per mole of $LaNi_{3.55}Co_{0.75}Mn_{0.4}Al_{0.3}$, F the Faraday (26 800 mAh), P_{H_2} the equilibrium hydrogen pressure, and E is the equilibrium potential of the hydride electrode.

The time interval between successive dehydriding steps in the electrochemical isotherms is critical. This interval should be long enough to ensure the attainment of equilibrium, but short enough to prevent the loss of hydrogen by self-discharge. The total time for a typical measurement was about 17 h. The influence of self-discharge on PCI measurements can be neglected since only 3.5% of the total hydrogen is desorbed within 17 h of self-discharge according to a parallel self-discharge measurement.

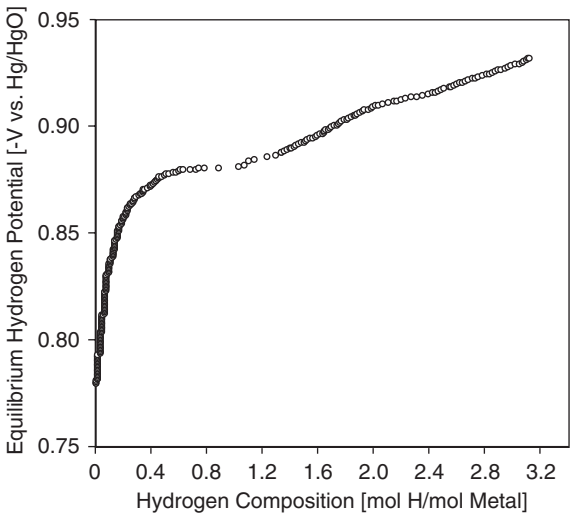

Fig. 1. Equilibrium potential-composition-isotherms (PCI) for the discharge of $LaNi_{3.55}Co_{0.75}Mn_{0.4}Al_{0.3}$ electrode in 6 M KOH + 0.5 M ZnO solution at 25 °C after 80 charge/discharge cycles.

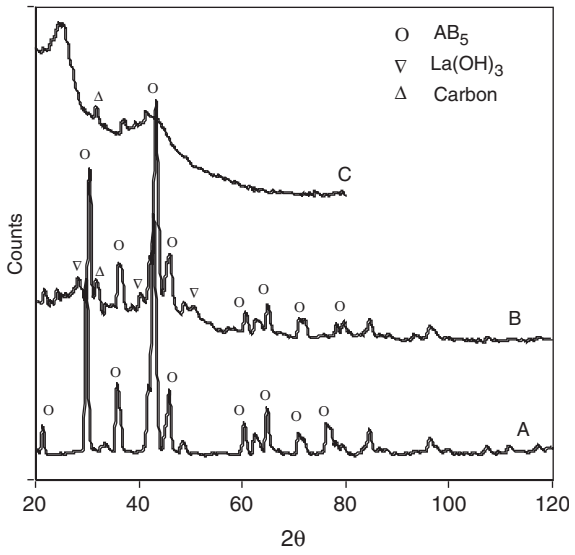

Fig. 2. X-ray diffraction patterns of the $LaNi_{3.55}Co_{0.75}Mn_{0.4}Al_{0.3}$ alloy. (a) Before charge/discharge cycles. (b) After 115 charge/discharge cycles in 6 M KOH + 0.5 M ZnO. (c) The alloy mixed with carbon.

2.3. Self-discharge of $LaNi_{3.55}Co_{0.75}Mn_{0.4}Al_{0.3}$

The self-discharge of the alloy $LaNi_{3.55}Co_{0.75}Mn_{0.4}Al_{0.3}$ was measured in both open and partially sealed cell configurations. Partial sealing of the cell is accomplished by simply capping the open cell, after the PCI curve was obtained, the electrode was fully recharged. The variation of the open-circuit potential (OCP) of the $LaNi_{3.55}Co_{0.75}Mn_{0.4}Al_{0.3}$ electrode as a function of time was then monitored at room temperature. The OCP-vs.-time plot was converted into composition–time plots according to the equilibrium potential-composition curves of $LaNi_{3.55}Co_{0.75}Mn_{0.4}Al_{0.3}$. The hydrogen desorption (self-discharge) rate at various times was obtained by taking the derivative of the composition–time plots. The PCI and OCP-rest time plots were used to derive the relationship between the hydrogen desorption rate, the hydrogen pressure, and the hydrogen content. Such relationship is vital in the study of the self-discharge mechanism of the hydride electrode.

3. Results and discussion

3.1. Self-discharge mechanism of $LaNi_{3.55}Co_{0.75}Mn_{0.4}Al_{0.3}$ electrodes in 6 M KOH + 0.5 M ZnO

The PCI for the discharge of the $LaNi_{3.55}Co_{0.75}Mn_{0.4}Al_{0.3}$ electrode (considered as a pseudobinary system) in 6 M KOH + 0.5 M ZnO were measured after 80 charge/discharge cycles. The results, shown in Fig. 1, indicate that hydrogen was readily released from the hydride–hydrogen solid solution phase in view of the gradual decrease in the pressure at the hydride phase with decreasing hydrogen content. Below 0.883 V (~ 1.4 H/M, the hydrogen-to-metal mole ratio in the MH electrode), the hydride phase transforms to the alloy as shown by the pressure (or potential) plateau in the PCI. The XRD patterns in Fig. 2 reveal that the $LaNi_{3.55}Co_{0.75}Mn_{0.4}Al_{0.3}$ alloy is in a $CaCu_5$-type hexagonal phase.

To obtain the self-discharge rate, the time-dependence of the OCP of the $LaNi_{3.55}Co_{0.75}Mn_{0.4}Al_{0.3}$ electrode was measured. The results are displayed in Fig. 3. The methods to measure and calculate the hydrogen evolution, oxidation, and phase transformation in Fig. 3 will be discussed in the sections that follow. During 600 h of open-circuit storage, the potential increased from −0.93 to −0.883 V, remained stable for a short period at about −0.883 V, and finally dramatically increased further. Based on the thermal desorption spectra of hydride electrodes at different rest times [5–7], it was concluded that these potential changes are due to the desorption of hydrogen from the MH electrode. Such desorption is driven by the difference between the partial pressure of hydrogen in the cell and the equilibrium hydrogen pressure at the MH electrode. As noted earlier, a more detailed mechanism is necessary to account for the complex trends of the experimental data.

The desorption of hydrogen from the hydride electrodes in an open-circuit cell may occur in four consecutive steps;

Step 1: Transformation from the hydride (β) to the metal–solution (α) phase:

$$MH_{x(\beta)} \longrightarrow MH_{x-y(\alpha)}. \quad (3)$$

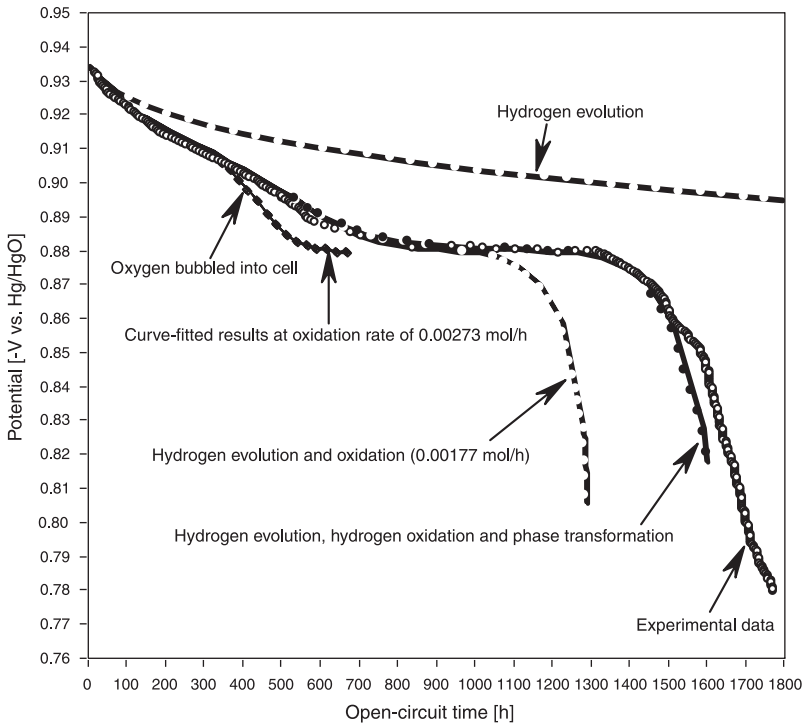

Fig. 3. OCP–time profile of $LaNi_{3.55}Co_{0.75}Mn_{0.4}Al_{0.3}$ electrode in 6 M KOH + 0.5 M ZnO solution with and without bubbled oxygen. The calculated OCP-vs.-time data based on: (i) hydrogen evolution only, (ii) hydrogen evolution and oxidation, (iii) hydrogen evolution plus oxidation and phase transformation, and (iv) oxygen bubbling are also shown for comparison.

Step 2: Diffusion of absorbed hydrogen from the bulk to the near-surface region:

$$MH_{bulk} \xrightarrow{\text{diffusion}} MH_{abs}. \quad (4)$$

Step 3: Reversible transfer of hydrogen from absorption sites in the near-surface region to adsorption sites on the electrode surface.

$$MH_{abs} \Leftrightarrow MH_{ads}. \quad (5)$$

Step 4: Combination of adsorbed hydrogen atoms into hydrogen gas:

$$MH_{ads} + MH_{ads} \rightarrow M + H_2. \quad (6)$$

The self-discharge rate is controlled by the slowest step. It has been demonstrated that the self-discharge behavior is independent of both the type (AB_2 or AB_5) of alloy and the thickness of the Cu coating [6]. Since it is well known that hydrogen diffusivity varies with these two parameters [6], it can thus be concluded that hydrogen diffusion is not the rate-limiting step of the self-discharge.

If hydrogen evolution were the controlling step of self-discharge, the rate should be proportional to the pressure difference between the partial pressure of hydrogen in the cell and the equilibrium hydrogen pressure at the hydride electrode [11]. From the experimental data presented in Figs. 1 and 3, we obtained the hydrogen desorption rate at different hydrogen pressures as follows. Since OCP is considered as the equilibrium potential, we can determine the hydrogen content at different open-circuit times by converting the OCP in Fig. 3 to hydrogen content using the PCI data. Thus, a plot of the hydrogen content as a function of open-circuit time (Fig. 4) can be generated. From the derivative of the data points in Fig. 4, the hydrogen desorption rate at different times are obtained (Fig. 5).

The use of Eq. (2) and the OCP-vs.-time data in Fig. 3 allows the transformation of the time axis in Fig. 5 to equilibrium pressure of hydrogen. Fig. 6 shows the hydrogen desorption rate at different equilibrium hydrogen pressures at the electrode, (dx/dP_{H_2}). The self-discharge rate (open-circles) has an almost linear dependence with the hydride electrode pressure, except for a small spike at 0.026 atm (0.884 V) where the hydride phase transforms into the alloy. The near-linear curve within the hydride phase (solid–solution) region suggests that the self-discharge rate depends on the equilibrium pressure of the hydride electrode because a hydrogen partial pressure of 10^{-7} atm in the open cell is essentially zero [7]. To probe the origin of this unusual (albeit small) behavior, the derivative of the

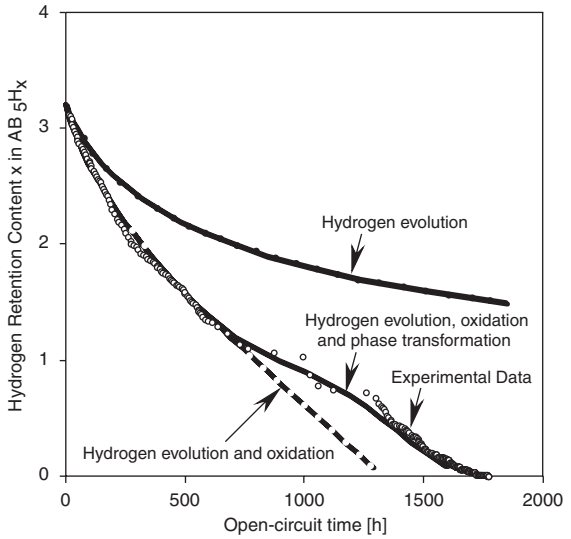

Fig. 4. Measured and calculated hydrogen content with open-circuit time for $LaNi_{3.55}Co_{0.75}Mn_{0.4}Al_{0.3}$ electrode in 6 M KOH + 0.5 M ZnO solution.

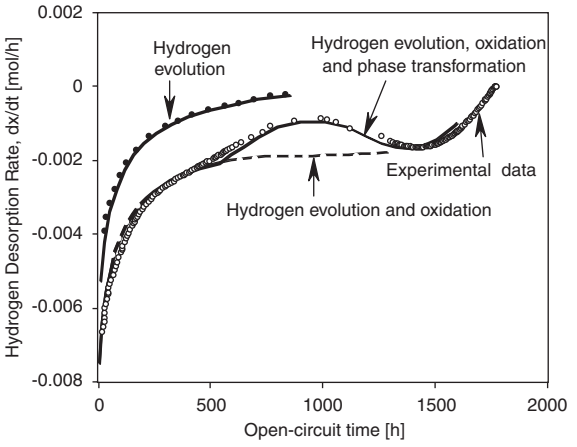

Fig. 5. Measured and calculated hydrogen desorption rate as a function of time for $LaNi_{3.55}Co_{0.75}Mn_{0.4}Al_{0.3}$ electrode in 6 M KOH + 0.5 M ZnO solution.

equilibrium pressure–composition curve, obtained by converting equilibrium potential in Fig. 1 to equilibrium hydrogen pressure P_{H_2} using Eq. (2), $(dx_{(PCI)}/dP_{H_2})$, was calculated and displayed in Fig. 6.

As earlier stated, in the potential range from −0.930 to −0.884 V (0.026 atm), hydrogen exists in the hydride phase as a solid solution. When the electrode potential increases above −0.884 V, the hydride begins to transform to the alloy (cf., Fig. 1). It is interesting to note that the peaks of the (dx/dP_{H_2}) and $(dx_{(PCI)}/dP_{H_2})$ plots are at the same pressure (potential) value. This suggests that the peak in the

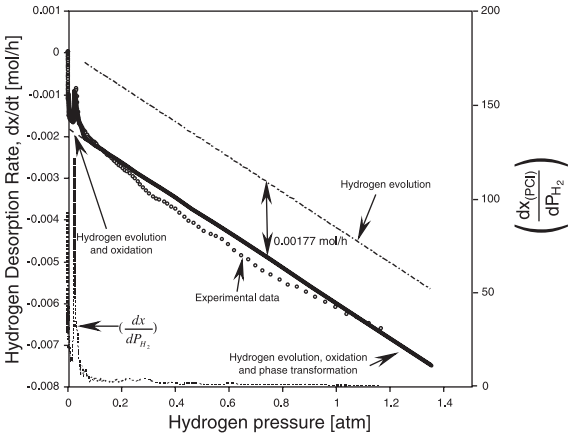

Fig. 6. Measured and calculated hydrogen desorption rate as a function of the equilibrium hydrogen pressure at the $LaNi_{3.55}Co_{0.75}Mn_{0.4}Al_{0.3}$ electrode in 6 M KOH + 0.5 M ZnO solution.

self-discharge rate in the phase-transformation region is induced by the slower phase-transformation rate rather than the hydrogen-evolution rate. The rate-controlling step for self-discharge is different from the rate-limiting step for the rate capability of the MH. It is well known that the limiting step for the rate capability is the diffusion of hydrogen into the MH rather than on the phase transformation. The reasons are as follows: (i) The overpotential of a MH electrode at self-discharge is quite small but becomes rather large if the electrode is charged/discharged at high current density. (ii) The increase in the rate of phase transformation is much faster than the enhancement of hydrogen diffusion brought about by an increase in the over-potential; this results in the changing of the limiting step from phase transformation to hydrogen diffusion as the charge–discharge current is increased. Hence, in a normal power tool (or HEV NiMH cell), phase transformation can allow discharge rates as high as 10 or 15 °C.

If the self-discharge rate in the single-hydride phase (at potentials below −0.884 V) depends only on the pressure difference between that at the hydride electrode and the hydrogen partial pressure (10^{-7} atm), the self-discharge rate can be calculated using the following equations:

$$\frac{d\chi_i}{dt_i} = k[P_{H_2}(\chi_i) - P_p] = 4.2 \times 10^{-3} \times P_{H_2}(\chi_i), \quad (7)$$

$$t_H(\chi_i) = \int_{3.2}^{\chi_i} \frac{d\chi_i}{4.2 \times 10^{-3} P_{H_2}(\chi_i)}, \quad (8)$$

where k, equal to 4.2×10^{-3} mol/h atm, was obtained from the slope of the curve in Fig. 6, $P_p = 10^{-7}$ atm, $P_{H_2}(x_i)$ is the equilibrium (open-circuit) pressure of hydride electrode at a hydrogen mole fraction x_i. x_i is equal to 3.2 (H/M) at potential of −0.93 V (cf., Fig. 1). We combined $t_{H_2}(\chi_i)$ and $P_{H_2}(\chi_i)$ to determine $t_{H_2}(P_{H_2})$, the open-circuit time

as a function of the equilibrium hydrogen pressure. As indicated by the spittled line in Fig. 6, the calculated self-discharge rate in the hydride-phase region approaches zero as the hydrogen pressure drops to zero, which is different from the measured self-discharge values. The disparity (0.00177 mol/h) between the calculated and measured values displayed in Fig. 6 suggests that, in addition to hydrogen evolution, other factors affect the self-discharge of hydride electrodes.

It is well known that metals are oxidized by DO in solutions exposed to air; the oxidation rate is controlled by the oxygen concentration in the solution [12]. The XRD pattern of the electrode in Fig. 2 revealed a small peak related to $La(OH)_3$ after 115 charge–discharge cycles in 6 M KOH + 0.5 M ZnO solution, which confirms that the $LaNi_{3.55}Co_{0.75}Mn_{0.4}Al_{0.3}$ is oxidized during 115 charge–discharge cycles. DO may also oxidize hydrogen adsorbed on the metal surface. If the oxidation reaction is controlled by oxygen diffusion, the oxidation rate of hydrogen is constant during self-discharge because, under open-cell conditions, the solution becomes saturated with oxygen; the DO concentration is constant (6–8 ppm by weight) and is independent of pH changes [13].

The rate of hydrogen oxidation due to DO at ambient conditions is estimated to be 0.00177 mol/h from Fig. 6. To ensure that the hydrogen oxidation rate was controlled by oxygen content, oxygen was bubbled into the cell [12] at an open-circuit time of 300 h. The experimental data show that bubbling oxygen into the cell increases the self-discharge rate. Oxygen bubbling increases the hydrogen oxidation rate from 0.00177 to 0.00273 mol/h. Fig. 3 shows how the results from the bubbling experiment coincided with the curve-fitted data. The regression line implies that the oxidation of hydrogen is another important factor that affects the self-discharge behavior. The occurrence of hydrogen desorption at a very low pressure of 10^{-8} atm (even lower than the hydrogen partial pressure in air, 10^{-7} atm) [7] can be explained by hydrogen oxidation.

Taking into account both hydrogen evolution and hydrogen oxidation, we can rewrite Eq. (8) as

$$t_{HO}(\chi_i) = \int_{3.2}^{\chi_i} \frac{d\chi_i}{4.2 \times 10^{-3} P_{H_2}(\chi_i) + 0.00177}. \quad (9)$$

The relation between OCP and time can be calculated by combining $t_{HO}(x_i)$ in Eq. (9), and $P_{H_2}(x_i)$. The calculated results are shown as a series of dashed lines in Fig. 3. The latter reveals that the calculated curve fits well with the experimental self-discharge data in the single-hydride-region; large discrepancies, however, are observed within the phase-transformation region. From Fig. 5, it can be seen that the self-discharge rate slows down within the two-phase region. It is possible that the nucleation and growth of the α phase from hydride β phase at the phase-transformation region (hydrogen content range of $x = 0$–1.4) limit the self-discharge rate. The hydrogen desorption rate

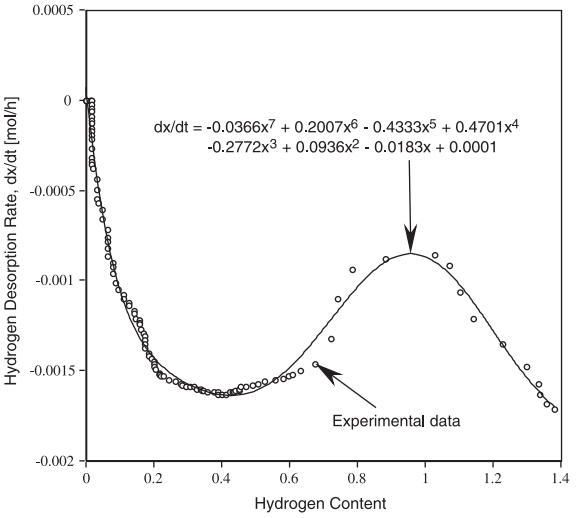

Fig. 7. Hydrogen desorption rate-vs.-hydrogen content in the phase-transformation region of $LaNi_{3.55}Co_{0.75}Mn_{0.4}Al_{0.3}$ in 6 M KOH + 0.5 M ZnO solution.

at the phase-transformation region can be curve-fitted using Eq. (10) (cf., Fig. 7):

$$Rz(\chi) = -0.0366\chi^7 + 0.2\chi^6 - 0.4333\chi^5 + 0.4701\chi^4 - 0.2772\chi^3 + 0.0936\chi^2 - 0.0183\chi + 0.00007, \quad (10)$$

where $Rz(x)$ is the hydrogen desorption rate at the electrode for a given hydrogen content, x. The time-composition expression for the phase-transformation region becomes,

$$t_{HOP}(\chi_i) = \int_{3.2}^{1.4} \frac{d\chi_i}{4.2 \times 10^{-3} P_{H_2}(\chi_i) + 0.00177} + \int_{1.4}^{\chi_i} \frac{d\chi_i}{Rz(\chi_i)} \quad (x_i \text{ from 0 to 1.4}). \quad (11)$$

The OCP-vs.-rest time plot can be re-calculated by combining Eqs. (2), (10), and (11) with $P_{H_2}(x_i)$. The solid line in Fig. 3 represents the recalculated values after consideration of the influence of hydrogen evolution, hydrogen oxidation, and phase transformation. It can be seen that the calculated open-circuit potentials agree quite well with the measured data.

From the above results, it is evident that the self-discharge behavior of the $LaNi_{3.55}Co_{0.75}Mn_{0.4}Al_{0.3}$ electrode is controlled by hydrogen evolution and hydrogen oxidation within the single-phase region ($x > 1.4$). Hydrogen evolution is induced by the difference between the partial pressure of hydrogen inside the cell and the equilibrium hydrogen pressure at the MH electrode, whereas hydrogen oxidation is brought about by DO. Within the two-phase region ($0 < x < 1.4$), the nucleation and growth of the solid-solution phase from the hydride phase is the rate-determining step of the

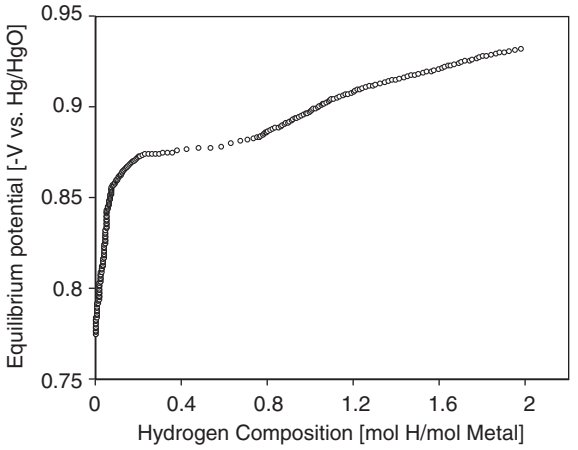

Fig. 8. Equilibrium potential-composition-isotherms (PCI) for the discharge of the $LaNi_{3.55}Co_{0.75}Mn_{0.4}Al_{0.3}$ electrode in 6 M KOH solution after 80 charge/discharge cycles.

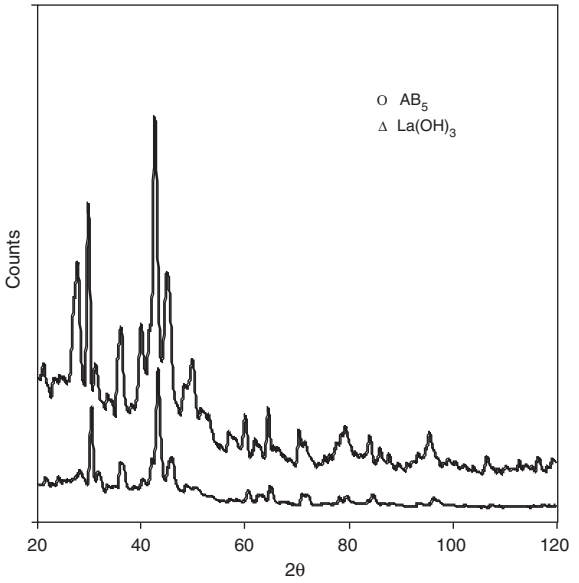

Fig. 9. X-ray diffraction patterns of the $LaNi_{3.55}Co_{0.75}Mn_{0.4}Al_{0.3}$ alloy mixed with carbon after 115 charge/discharge cycles in 6 M KOH solution.

self-discharge mechanism. The present self-discharge mechanism for hydride electrodes can be used to explain the experimental results reported by elsewhere [5–7].

3.2. *Effect of sealed cells and* ZnO *on the self-discharge characteristics*

Eq. (7) shows that the facility of hydrogen evolution is not only controlled by pressure differences, ΔP, but also influenced by the coefficient k, which represents a resistance for hydrogen evolution from the hydride electrode. In this study, the cell was (loosely) capped to increase the resistance against hydrogen escape. The effect of ZnO on hydrogen oxidation was also investigated; we describe here the results of the self-discharge of $LaNi_{3.55}Co_{0.75}Mn_{0.4}Al_{0.3}$ in 6 M KOH without ZnO using a partially sealed cell in comparison with earlier studies of the same alloy in 6 M KOH + 0.5 M ZnO using an open cell.

Fig. 8 shows the equilibrium potential composition of the $LaNi_{3.55}Co_{0.75}Mn_{0.4}Al_{0.3}$ electrode in 6 M KOH after 80 cycles. As expected, the resulting discharge capacity of the alloy in ZnO-free KOH is lower than the ZnO-containing solution (Figs. 1 and 8). XRD patterns reveal that, after 115 cycles, the $La(OH)_3$ peak of the alloy in 6 M KOH is higher than that in the solution containing 0.5 M ZnO in 6 M KOH (cf., Figs. 2 and 9). The presence of ZnO in alkaline solution is thus shown to inhibit the corrosion of $LaNi_{3.55}Co_{0.75}Mn_{0.4}Al_{0.3}$ during charge/discharge cycles.

The OCP–time profile of the $LaNi_{3.55}Co_{0.75}Mn_{0.4}Al_{0.3}$ electrode in a partially sealed cell with 6 M KOH is shown in Fig. 10. Using the same procedure as in previous cases, the hydrogen retention at different times was determined (Fig. 11). Fig. 12 displays a plot of the hydrogen-desorption rate at various equilibrium pressures at the alloy. From these data, the coefficient k was calculated. In the absence of

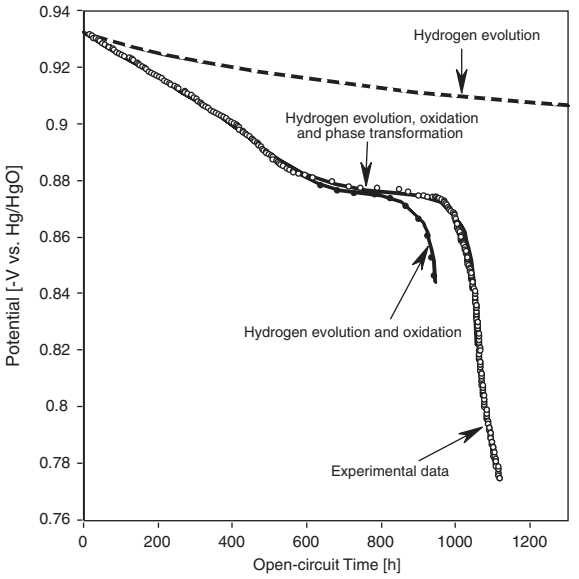

Fig. 10. Measured and calculated OCP–time profile for the $LaNi_{3.55}Co_{0.75}Mn_{0.4}Al_{0.3}$ electrode in 6 M KOH solution.

ZnO, the calculated k was 1.95×10^{-3} mol/h atm, which is smaller than that in 6 M KOH + 0.5 M ZnO solution, 4.2×10^{-3} mol/h atm. It can be argued that the self-discharge rate of the MH electrode in the partially sealed cell is smaller than in an open cell. It can also be seen in Fig. 12 that the hydrogen-oxidation rate in 6 M KOH (0.00167 mol/h) is

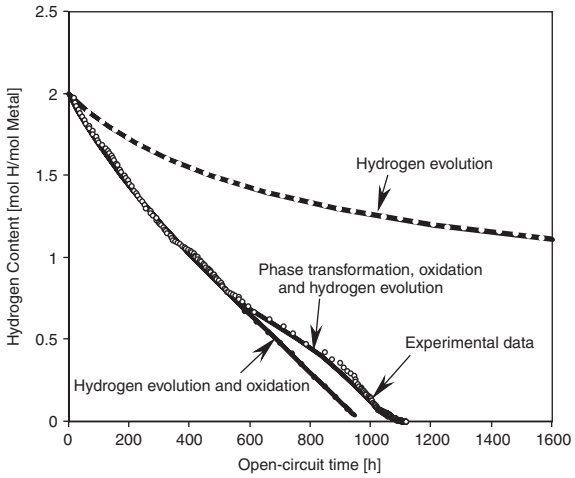

Fig. 11. Measured and calculated hydrogen content with respect to open-circuit time for $LaNi_{3.55}Co_{0.75}Mn_{0.4}Al_{0.3}$ in 6 M KOH solution.

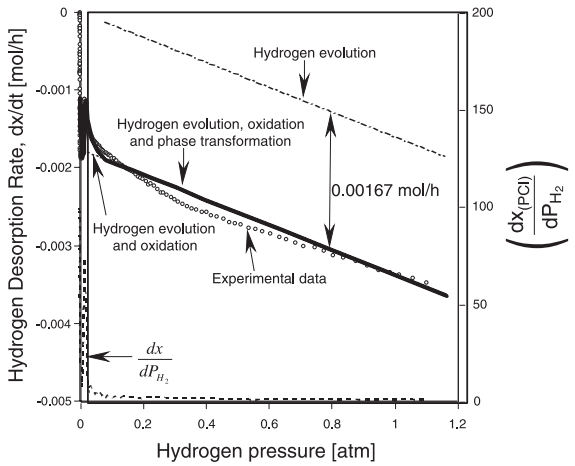

Fig. 12. Measured and calculated hydrogen desorption rates as functions of the equilibrium hydrogen pressure at the $LaNi_{3.55}Co_{0.75}Mn_{0.4}Al_{0.3}$ electrode in 6 M KOH solution.

only slightly smaller than that in 6 M KOH + 0.5 M ZnO (0.00177 mol/h). The small difference may be due to the low concentration of oxygen in the partially sealed cell. ZnO does not appear to enforce an obvious effect on hydrogen oxidation since similar oxidation rates were obtained from alkaline solutions in the presence or absence of ZnO .

The phase-transformation rate for $LaNi_{3.55}Co_{0.75}Mn_{0.4}Al_{0.3}$ in 6 M KOH was curve-fitted with Eq. (12).

$$R(\chi) = -1.4709\chi^7+5.0407\chi^6-6.9193\chi^5+4.8822\chi^4 - 1.9023\chi^3+0.4096\chi^2-0.0438\chi-0.0001. \quad (12)$$

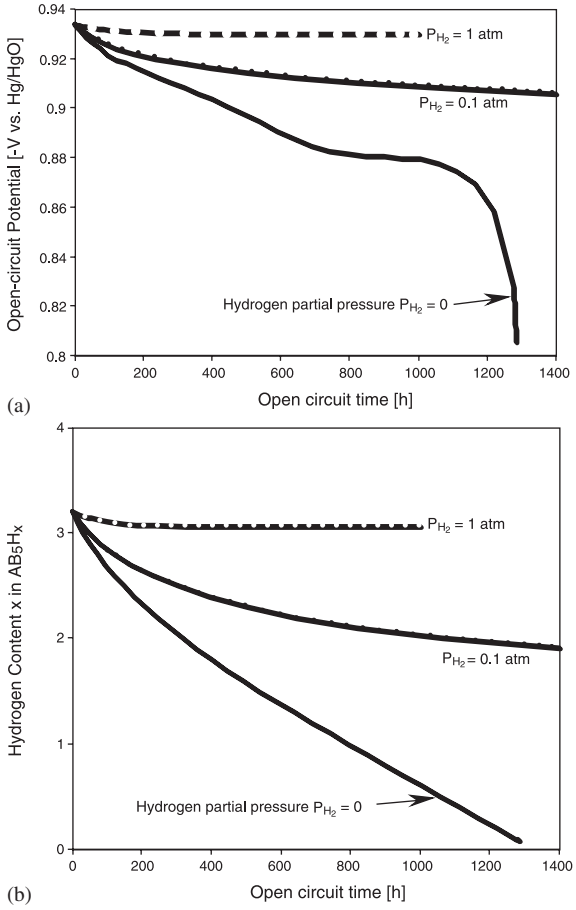

Fig. 13. The effect of partial pressure of hydrogen on: (a) the open-circuit potential and (b) the hydrogen content for $LaNi_{3.55}Co_{0.75}Mn_{0.4}Al_{0.3}$ in 6 M KOH.

Calculated curves obtained by consideration of hydrogen evolution, hydrogen oxidation, and phase transformation are also shown in Figs. 10–12. The close agreement of the calculated and experimental curves supports the proposed self-discharge mechanism.

3.3. Effect of partial pressure of hydrogen in the cell on the self-discharge characteristics

The data presented in the previous sections clearly demonstrate the influence of hydrogen evolution and oxidation on the self-discharge behavior of $LaNi_{3.55}Co_{0.75}Mn_{0.4}Al_{0.3}$ in the single-phase region. It is expected that reduction of the driving forces of hydrogen evolution and oxidation will reduce the extent of self-discharge.

Fig. 13 shows the simulated effects of the partial pressure of hydrogen on the OCP and hydrogen retention. It can be seen that the self-discharge rate decreases quickly as the hydrogen pressure in the cell is increased from 0 to 1 atm.

Similar results were reported in other studies that probed the effects of air and H_2 [6]; it was found that the charge retention was improved significantly upon application of 1 atm of hydrogen.

4. Conclusions

A new method of measuring the self-discharge rate of MH electrodes has been developed. From the equilibrium potential-composition-isotherms (PCI) of the hydrogen desorption of the $LaNi_{3.55}Co_{0.75}Mn_{0.4}Al_{0.3}$ electrode, and open-circuit potential (OCP)-vs.-time measurements, the self-discharge behavior at different equilibrium pressures was evaluated. In the mechanism proposed here, the self-discharge of $LaNi_{3.55}Co_{0.75}Mn_{0.4}Al_{0.3}$ within the single-phase region is attributed to hydrogen evolution and oxidation. The difference between the partial pressure of hydrogen in the cell and the equilibrium hydrogen pressure at the hydride electrode is a critical factor in the occurrence of hydrogen evolution. Hydrogen oxidation is caused by DO in the alkaline solution. However, in the two-phase region, the self-discharge behavior is controlled by the rate of phase transformation from the hydride phase to the α phase. The self-discharge rate of the $LaNi_{3.55}Co_{0.75}Mn_{0.4}Al_{0.3}$ electrode in a partially sealed cell is lower than that in an open cell. Addition of ZnO into the alkaline solution has no obvious effect on self-discharge, although the corrosion of the $LaNi_{3.55}Co_{0.75}Mn_{0.4}Al_{0.3}$ electrode is inhibited. Simulations using the proposed self-discharge mechanism provide results that concur with the experimental (OCP) data. The calculated self-discharge rates at different hydrogen pressures are in agreement with previously reported results.

Acknowledgements

The work was performed under the auspices of the US Department of Energy, Division of Chemical Sciences, Office of Basic Energy Science (Contract no. DE-AC02-76CH00016, BNL and DE-FG03-93ER1481). M.P.S. would like to thank the Welch Foundation for additional partial support. The assistance of X. Chen is gratefully acknowledged.

References

[1] (a) Willems JJG. Philips. J Res 1984;39:1.
(b) Willems JJG, Buschow KHJ. J Less-Common Met 1987;129:13.
[2] Ikpma M, Hoshina Y, Matsumoto I, Iwakura C. J Electrochem Soc 1996;143:1904.
[3] Leblanc P, Blanchard P, Senyarich S. J Electrochem Soc 1998;145:844.
[4] Iwakura C, Kajiya Y, Yoneyama H, Sakai T, Oguro K, Ishikawa H. J Electrochem Soc 1989;136:1351.
[5] Lee JH, Lee KY, Lee SM, Lee JY. J Alloys Compounds 1995;221:174.
[6] Lee JH, Lee KY, Lee JY. J Alloys Compounds 1996;232:197.
[7] Jang KJ, Jung JH, Kim DM, Yu JS, Lee JY. J Alloys Compounds 1998;268:290.
[8] Wang C, Marrero-Cruz M, Soriaga MP, Serafini D, Srinivasan S. Electrochimica Acta 2002;47:1069.
[9] Wang C, Marrero-Cruz M, Baricuatro JH, Soriaga MP, Serafini D, Srinivasan S. J Appl Electrochem 2003;33:325.
[10] Wang C, Wang XH, Lei YQ, Chen CP, Wang QD. Int J Hydrogen Energy 1997;22:1117.
[11] Wang C, Wang XH, Lei YQ, Chen CP, Wang QD. Int J Hydrogen Energy 1996;21:471.
[12] Mukerijee SJ, McBreen J, Adzic C, Johnson JR, Reilly JJ, Marrero MR. et al. J Electrochem Soc 1997;144:L258.
[13] Scully JC. The fundamentals of corrosion. Oxford: Pergamon Press; 1990.